Computational optimal design of random rough surfaces in thin-film solar cells

Gang Bao[1], Yanzhao Cao[2] Junshan Lin[3,*]and Hans Werner Van Wyk [4]

[1] *Department of Mathematics, Zhejiang University, China.*
[2] *Department of Mathematics and Statistics, Auburn University, Auburn, AL 36849, U.S.A.*
[3] *Department of Mathematics and Statistics, Auburn University, Auburn, AL 36849, U.S.A.*
[4] *Department of Mathematics and Statistics, Auburn University, Auburn, AL 36849, U.S.A.*

Abstract. Random rough textures can increase the absorbing efficiency of solar cells by trapping the optical light and increasing the optical path of photons. In this paper, we are concerned with optimal design of random rough surfaces in thin-film solar cells. We formulate the design problem as a random PDE constrained optimization problem and employ gradient-based methods for solving the problem numerically. To evaluate the gradient of the objective function, the Monte-Carlo method is used for sampling the probability space and the adjoint state method is employed to calculate the gradient at each sample. Numerical examples are shown to test the efficiency of the proposed algorithm. It is demonstrated that optimally obtained random textures yield an enormous absorption enhancement and a higher photon absorptance than that of existing random textures.

AMS subject classifications: 35J05, 35Q60, 49Q10, 65C05, 65C30

Key words: Optimal design, random rough surface, solar cell, Helmholtz equation.

1 Introduction

Photovoltaics (PV), which directly convert solar energy into electricity, offer a practical and sustainable solution to the challenge of meeting the increasing global energy demand. A typical photovoltaic system employs solar panels, each consisting a number of solar cells to generate electrical power from sun light that can be used to power equipment or to recharge a battery [21]. One representative cell configuration is the so-called

*Corresponding author. *Email addresses:* bao@math.zju.edu.cn. (G. Bao), yzc0009@auburn.edu (Y. Cao), jzl0097@auburn.edu (J. Lin), hzv0008@auburn.edu (H. Van Wyk)

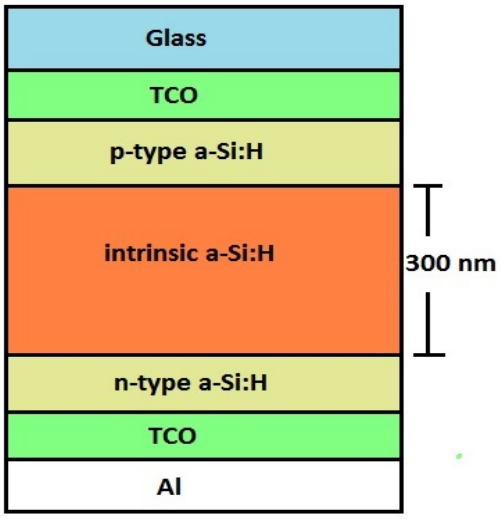

Figure 1: A schematic plot of thin-film solar cells.

thin-film solar cell, which is made of hydrogenated amorphous silicon (a-Si:H) and microcrystalline silicon (μc-Si:H). A typical a-Si:H cell structure is shown in Figure 1, where the intrinsic a-Si:H is the absorbing layer that has a thickness of a few hundred nanometers. Compared to traditional crystalline silicon solar cells, thin-film cells offer several distinctive features such as much smaller thickness, low cost in production, and special optical properties of a-Si:H and μc-Si:H [26].

The mass production of stable a-Si:H cells requires that the maximum thickness of their light absorbing layer is often limited to about 300 nm [26]. Such a layer is sufficiently absorptive at smaller optical wavelengths and all the incoming light in that frequency band can be effectively absorbed. However, at larger wavelengths (typically >600 nm), a-Si:H is poorly absorptive and most photon energy escapes. Consequently, the overall efficiencies of thin-film solar cells are low, and their optical structures have to be engineered in a way so as to increase the absorption and enhance their performance.

There exist various ways to increase the absorption efficiency of solar cells, for instance, antireflection coating, fluorescent dyes, dielectric gratings, photonic crystals, and plasmonic nanoparticles, etc [3, 4, 7, 13, 28]. However, it is still unclear whether such design will find their way into commercial photovoltaic devices because of their high costs. Another way to increase the efficiency of photon absorption is using randomly nanotextured interfaces to trap the optical light [1, 11, 12, 17, 27]. The randomly textured surfaces lower the reflection losses at the entrance facet and scatter the light, thereby increasing the optical path of each photon in the solar cell. In thin-film solar cells, this is usually achieved by texturing the surface of the transparent conductive oxide (TCO) layer as shown in Figure 1 (see also [22]). Very importantly, in practice the control and fabrication of the TCO interface in a random manner can be achieved at very low cost by controlling the deposition parameter of TCO films sputtered on glass substrates [18, 23]. Such cost-effective feature offers significant advantages in real fabrications compared to other

structures. Thus commercialized cells of this sort, such as the Asahi-U substrate, the Jülich substrate, and the Neuchătel substrate, have been developed. Meanwhile, to increase the absorption efficiency, numerical studies have also been carried out to optimize the randomness of TCO layer surfaces [11, 12, 17, 27]. The readers are referred to [19, 29] and references therein for the optimal design of deterministic textures in solar cells [†]. We also refer to [8, 9, 14, 15, 30] for other deterministic shape optimization problems that arise in physics and engineering.

Previous studies on the optimization of random textures are mostly performed by certain ad hoc procedures [11, 12, 17, 27]. They involve computing the absorptance for several chosen statistical parameters and then choosing the ones that yield the largest absorptance among all computed values. Such ad hoc schemes are computationally inefficient. Furthermore, the obtained optimal solutions heavily depend on the set of statistical parameters being chosen, and the real global optimal statistical parameters that yield the highest solar absorptance can easily fall out of this set. In this paper, we formulate the optimal design of random surface textures as a random PDE constrained problem. The gradient-based algorithm is applied to solve the random optimization problem, and for obtaining the statistical parameters of the optimal random textures. In order to evaluate the gradient of the objective function, the Monte-Carlo method is used for sampling the probability space and the adjoint state method is applied for computing the gradient at each sample. It is demonstrated that new random textures give rises to a significant absorption enhancement and their photon absorptance is higher than that of existing random textures.

The rest of the paper is organized as follows. In Section 2 we introduce the mathematical model for the optical scattering problem by random rough surfaces. The optimal design problem is formulated in Section 3, and the computation of the shape derivative and the gradient for the cost function is elaborated. Several numerical experiments are presented in Section 4 to demonstrate the efficiency of the numerical method, followed by several general concluding remarks.

2 Mathematical formulation

2.1 Optical scattering problem

We consider the two-dimensional model as depicted in Figure 2, by assuming that the cell is invariant along the x_3 direction. Since the goal is to optimize the random textures for the TCO layer, and the index contrast between the glass substrate and the TCO is rather low, for simplicity we don't explicitly consider glass substrate and assume that the cell consists of two layers only. That is, an absorbing layer (e.g., a-Si:H) sits at the

[†]It should be pointed out that, although typically the overall efficiency of the optimal deterministic interface would yield a higher absorption efficiency than the average absorption efficiency of random ones, the former may loose its attractiveness in real applications due to the high cost to fabricate the complete optimal structure.

bottom and a transparent conducting oxide (TCO) layer lies on the top. Let us denote the permittivity of the cell by $\varepsilon = \varepsilon_r \varepsilon_0$, where ε_0 is the permittivity in the vacuum and ε_r is the relative permittivity value. The absorbing layer and the TCO layer attain a relative permittivity value of $\varepsilon_{r,1}$ and $\varepsilon_{r,2}$, respectively. The interface between the two layers is textured in a random manner. Let Ω be the sample space. For each random sample $\omega \in \Omega$, we define $\Gamma(\omega) := \{(x_1, x_2) \mid x_2 = f(\omega; x_1)\}$ and denote the random interface by $\Gamma(\omega)$. The cell is closed with a perfect reflector at the bottom, thus no transmission of the optical light occurs. It is also assumed that the whole structure is periodic with the size of the period Λ. Then in the reference period $D_\Lambda := (0, \Lambda) \times \mathbb{R}^+$, the domains for the TCO and absorbing layers are given by

$$D_1(\omega) := \{(x_1, x_2) \mid x_1 \in (0, \Lambda), 0 < x_2 < f\}$$

and

$$D_2(\omega) := \{(x_1, x_2) \mid x_1 \in (0, \Lambda), f < x_2 < \infty\}$$

respectively.

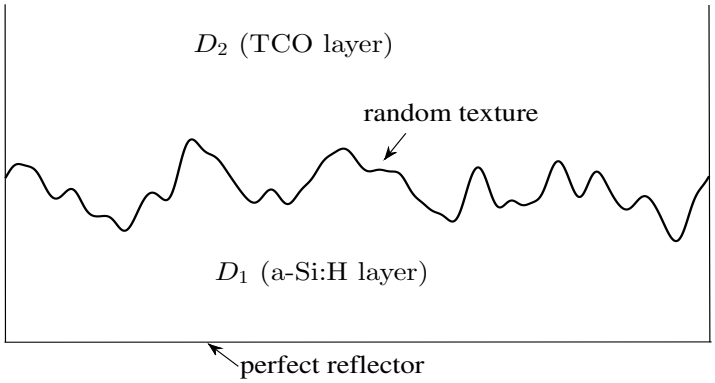

Figure 2: Schematic plot of the geometry.

We consider the transverse electric (TE) case for which the electric field $E = (0, 0, u)$. The random structure is illuminated by an incident time–harmonic plane wave $u^i = e^{ik_0 q_2 d \cdot x}$, where k_0 is the free-space wavenumber, $q_2 (:= \sqrt{\varepsilon_{r,2}})$ is the refractive index of the TCO layer, and d is the propagation direction. For clarity of presentation, we restrict the discussion of the optimal design under the normal incidence, or $d = [0, -1]^T$. The mathematical formulation and numerical algorithm introduced here can be extended straightforwardly to the case of the oblique incidence. The total field u after the scattering consists of the incident wave u^i and the scattered wave u^s. For each sample ω, it satisfies

$$\begin{cases} \Delta u(\omega; \cdot) + k_0^2 \varepsilon_r u(\omega; \cdot) = 0 & \text{in } D_\Lambda \backslash \Gamma(\omega), \\ u(\omega; 0, x_2) = u(\omega; \Lambda, x_2), \\ u(\omega; x_1, 0) = 0, \quad 0 < x_1 < \Lambda, \end{cases} \tag{2.1}$$

where the relative permittivity

$$\varepsilon_r = \begin{cases} \varepsilon_{r,1}, & x_2 < f(\omega;x_1), \\ \varepsilon_{r,2}, & x_2 > f(\omega;x_1). \end{cases}$$

Along the surface $\Gamma(\omega)$, the continuity of the electric field and magnetic field implies that

$$u_+(\omega;x_1,f(\omega,x_1)) = u_-(\omega;x_1,f(\omega,x_1)), \tag{2.2}$$
$$\partial_\nu u_+(\omega;x_1,f(\omega,x_1)) = \partial_\nu u_-(\omega;x_1,f(\omega,x_1)), \tag{2.3}$$

where ν denotes the unit normal vector along $\Gamma(\omega)$ pointing toward $D_2(\omega)$, $u_\pm$ and $\partial_\nu u_\pm$ denote the limits of u and $\partial_\nu u$ from above and below the surface respectively. In addition, the scattered field u^s is outgoing in the domain $D_2(\omega)$ that lies above the interface $\Gamma(\omega)$ [2,5].

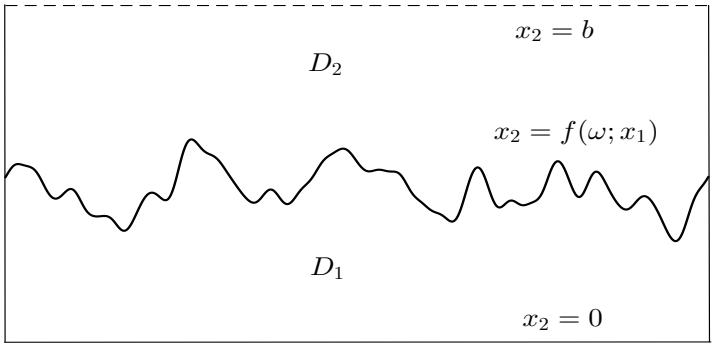

Figure 3: Scattering problem in the bounded domain $D := \{(x_1,x_2) \,|\, 0 < x_1 < \Lambda, 0 < x_2 < b\}$.

To formulate the scattering problem in a bounded domain, let us introduce the Dirichlet-to-Neumann map on the line $x_2 = b > \max f$ (cf. Figure 3, [2]). For a fixed sample ω, by virtue of the well-known Rayleigh expansion, the scattered field above $\Gamma(\omega)$ can be expressed as

$$u^s(\omega;\cdot) = \sum_{n=-\infty}^{\infty} \hat{u}_n^s(\omega;b)\, e^{i\kappa_n x_1 + i\eta_n (x_2 - b)}, \tag{2.4}$$

where $\kappa_n := \dfrac{2\pi n}{\Lambda}$ for $n \in \mathbb{Z}$ and

$$\eta_n = \begin{cases} \sqrt{k_0^2 \varepsilon_{r,2} - \kappa_n^2}, & k > \kappa_n, \\ \\ i\sqrt{\kappa_n^2 - k_0^2 \varepsilon_{r,2}}, & k < \kappa_n. \end{cases} \tag{2.5}$$

$\hat{u}_n^s(\omega;b)$ are the Fourier coefficients of $u^s(\omega;x_1,b)$ defined by

$$\hat{u}_n^s(\omega;b)=\frac{1}{\Lambda}\int_0^{\Lambda}u^s(\omega;x_1,b)e^{-i\kappa_n x_1}dx_1. \tag{2.6}$$

It then follows that for $x_2=b$,

$$\frac{\partial u^s}{\partial x_2}(\omega;x_1,b)=\sum_{n=-\infty}^{\infty}i\eta_n\hat{u}_n^s(\omega;b)e^{i\kappa_n x_1}=:T[u^s(\omega;x_1,b)]. \tag{2.7}$$

By notating that $u=u^i+u^s$ and following a direct calculation, we obtain

$$\frac{\partial u}{\partial x_2}(\omega;x_1,b)=T(u(\omega;x_1,b))+g,$$

where $g=-2ik_0q_2e^{-ik_0q_2b}$. Therefore, for each sample ω, the scattering problem can be formulated in a bounded domain D as

$$\begin{cases}\Delta u(\omega;\cdot)+k_0^2\varepsilon_r u(\omega;\cdot)=0 & \text{in } D\backslash\Gamma(\omega),\\ u(\omega;0,x_2)=u(\omega;\Lambda,x_2), & 0<x_2<b,\\ u(\omega;x_1,0)=0, & 0<x_1<\Lambda\\ \dfrac{\partial u}{\partial x_2}(\omega;x_1,b)=T(u(\omega;x_1,b))+g & 0<x_1<\Lambda.\end{cases} \tag{2.8}$$

Additionally, the continuity conditions (2.2) - (2.3) are imposed along the interface $\Gamma(\omega)$.

2.2 Modeling of random surfaces

Let $x_2=a$ be the reference surface with the height $a>0$. The random texture profile is represented as

$$f(\omega;x_1)=a+h(\omega;x_1),$$

where $h(\omega;x_1)$ is the deviation of the random surface from the reference surface. It is assumed that $h(\omega;x_1)$ is a stationary Gaussian process with zero mean and a continuous and bounded covariance $C(x_1,y_1)=c(x_1-y_1)$. Two widely used covariance functions for the modeling of rough surfaces are

$$c(x_1-y_1)=\sigma^2\exp(-|x_1-y_1|^q/\ell^q)\quad \text{for } q=1,2,$$

where σ is the root mean square (RMS) height of the surface and ℓ is the correlation length [25]. Here we consider the Gaussian type correlation by letting $q=2$ and $0<\ell\ll\Lambda$.

We adopt the well–known Karhunen–Loève expansion to represent the random process $h(\omega;x_1)$ [20]. In more detail, since $h(\omega;x_1)$ is Λ-periodic, we may expand its covariance function $c(x_1)$ as a Fourier series. By noting that $c(x_1)$ is even, it follows that

$$c(x_1)=\sigma^2\left[\frac{\hat{c}_0}{2}+\sum_{p=1}^{\infty}\hat{c}_p\cos\left(\frac{2p\pi x_1}{\Lambda}\right)\right],$$

where $\hat{c}_0, \hat{c}_1, \hat{c}_1, \cdots$ are the Fourier cosine expansion coefficients of the correlation function $\exp(-|x_1-y_1|^2/\ell^2)$. It can be shown explicitly that the covariance operator

$$K\varphi(x_1) := \int_0^\Lambda c(x_1-y_1)\,\varphi(y_1)dy,$$

possesses the eigenvalues

$$\lambda_j = \frac{\sigma^2\Lambda\hat{c}_j}{2}, \quad j=0,1,2,\cdots.$$

The corresponding eigenfunctions are

$$\varphi_j(x_1) = \begin{cases} \sqrt{\dfrac{1}{\Lambda}}, & j=0, \\ \sqrt{\dfrac{2}{\Lambda}}\cos\left(\dfrac{2j\pi x_1}{\Lambda}\right), & j>1,\text{even} \\ \sqrt{\dfrac{2}{\Lambda}}\sin\left(\dfrac{2j\pi x_1}{\Lambda}\right), & j>1,\text{odd}. \end{cases}$$

The Karhunen–Loève representation of the random process $h(\omega;x_1)$ is given by

$$h(\omega;x_1) = \sqrt{\lambda_0}\xi_0(\omega)\sqrt{\frac{1}{\Lambda}} + \sum_{j=1}^{\infty}\sqrt{\lambda_j}\left[\xi_{j,s}(\omega)\sqrt{\frac{2}{\Lambda}}\sin\left(\frac{2j\pi x_1}{\Lambda}\right) + \xi_{j,c}(\omega)\sqrt{\frac{2}{\Lambda}}\cos\left(\frac{2j\pi x_1}{\Lambda}\right)\right], \tag{2.9}$$

where ξ_0, $\xi_{j,c}$ and $\xi_{j,s}$ are *i.i.d.* Gaussian random variables with zero mean and unit covariance.

Alternatively, by letting

$$\lambda_j = \sigma^2\bar{\lambda}_j \quad \text{where}\,\bar{\lambda}_j = \frac{\Lambda\hat{c}_j}{2},$$

we may express the profile of the random surface by

$$h(\omega;x_1) = \sigma\cdot\bar{h}(\omega;x_1), \tag{2.10}$$

where

$$\bar{h}(\omega;x_1) = \sqrt{\bar{\lambda}_0}\xi_0(\omega)\sqrt{\frac{1}{\Lambda}} + \sum_{j=1}^{\infty}\sqrt{\bar{\lambda}_j}\left[\xi_{j,s}(\omega)\sqrt{\frac{2}{\Lambda}}\sin\left(\frac{2j\pi x_1}{\Lambda}\right) + \xi_{j,c}(\omega)\sqrt{\frac{2}{\Lambda}}\cos\left(\frac{2j\pi x_1}{\Lambda}\right)\right].$$

It is clear that $\bar{h}$ is independent of the RMS height σ.

In practical computations, a finite–term Karhunen–Loève expansion is adopted such that the contribution from the truncated terms is negligibly small. Figure 4 shows the decay of the eigenvalues $\bar{\lambda}_j$ when the period is $\Lambda=1$ and the correlation length is $\ell=0.02$. We see that the first 50 terms of the Karhunen–Loève expansion to represent $\bar{h}$ would give an accuracy of about 10^{-3}.

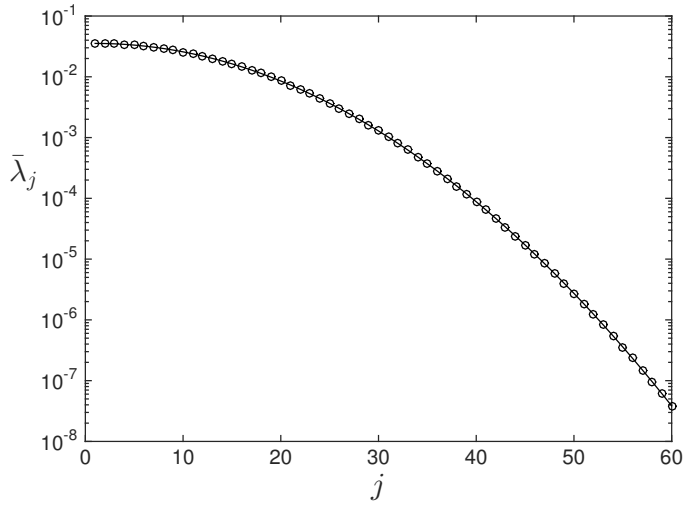

Figure 4: Eigenvalues for the Gaussian covariance operator when $\Lambda = 1$ and $\ell = 0.02$.

3 Optimal design of random rough surface

3.1 Optimal design problem

For each sample ω, let $R(\omega)$ and $A(\omega)$ denote the reflectivity in the TCO layer and the absorptance in the absorbing layer, respectively. From the conservation of energy, it is clear that

$$R(\omega) + A(\omega) = 1.$$

The optimal design problem seeks to maximize the mean absorptance $\mathbb{E}[A]$, or equivalently, to minimize the mean reflectivity $\mathbb{E}[R]$. To define the reflectivity $R(\omega)$, in light of the Rayleigh expansion (2.4), we rewrite the scattered field as

$$u^s(\omega;\cdot) = \sum_{n=-\infty}^{\infty} r_n(\omega)\, e^{i\kappa_n x_1 + i\eta_n x_2},$$

where the reflection coefficient $r_n(\omega) = \hat{u}_n^s(\omega;b)e^{-i\eta_n b}$, and $\hat{u}_n^s$ are the Fourier coefficients of the scattered field u^s as defined in (2.6). Alternatively, by a direct calculation, it can be shown that

$$r_n(\omega) = \begin{cases} \hat{u}_n(\omega;b)e^{-i\eta_n b}, & n \neq 0 \\ \hat{u}_n(\omega;b)e^{-ik_1 b} - e^{-2ik_1 b}, & n = 0, \end{cases} \tag{3.1}$$

where $\hat{u}_n(\omega;b)$ are the Fourier coefficients of the total field $u(\omega;\cdot)$ on the boundary $x_2 = b$.

Let $\mathcal{N} := \{n \in \mathbb{Z} \,|\, k_0^2 \varepsilon_{r,2} - \kappa_n^2 > 0\}$ be the set of indices for all propagating modes in the Rayleigh expansion. For each sample $\omega \in \Omega$, the reflectivity associated with the solar cell

is given by

$$R(\omega;f)=\sum_{n\in\mathcal{N}}\frac{\eta_n}{\eta_0}|r_n(\omega)|^2,$$

where η_n is defined in (2.5). Thus the mean reflectivity is

$$\mathbb{E}[R]:=\int_\Omega\sum_{n\in\mathcal{N}}\frac{\eta_n}{\eta_0}|r_n(\omega)|^2\,dP(\omega).$$

Recall that Ω and P denotes the random sample space and the probability measure, respectively.

Let $\alpha:=(\sigma,\ell)$ be a vector with two components. We define the cost function

$$J(\alpha):=\mathbb{E}[R(\omega,f)].$$

Then the optimal design problem is to minimize the mean reflectivity $J(\alpha)$, or equivalently, to solve the optimization problem

$$\min_{\alpha\in U_\alpha}J(\alpha) \tag{3.2}$$

over an admissible set $U_\alpha\subset\mathbb{R}^2$. In this paper, we apply the gradient-based method to solve the optimization problem (3.2). The Armijo's line search method is used to find a suitable step length [24]. To this end, the gradient of the cost function $\nabla_\alpha J$ needs to be calculated during each iteration. This is discussed in details in what follows.

3.2 Computation of the gradient $\nabla_\alpha J$

For each sample ω, by the chain rule, the gradient of $R(\omega;f(\alpha))$ is

$$\nabla_\alpha R=\nabla_f R\cdot\nabla_\alpha f.$$

$\nabla_f R$ is the shape derivative of R with respect to the surface (cf. [30]), and $\nabla_\alpha f$ is the gradient of f with respect to the statistical parameters α. The shape derivate is a key ingredient of any gradient based shape control algorithms (cf. [10]). Here the shape derivative $\nabla_\alpha R$ can be evaluated by the adjoint state approach (cf. [16]) and its formula is given in the following theorem.

Theorem 3.1. The gradient $\nabla_\alpha R$ can be expressed as

$$\nabla_\alpha R=\frac{2k_0^2}{\Lambda}\sum_{n\in\mathcal{N}}\frac{\eta_n}{\eta_0}\mathrm{Re}\Big[(\hat{u}_n(\omega;b)-\alpha_n e^{-ik_1 b})\cdot\overline{(\varepsilon_{r,1}-\varepsilon_{r,2})}\cdot\int_0^\Lambda[\bar{u}u_n^*]|_{(x_1,f)}\cdot\nabla_\alpha f\,dx_1\Big], \tag{3.3}$$

where $\alpha_0 = 1$ and $\alpha_n = 0$ if $n \neq 0$. u is the solution to the forward problem (2.8), and u_n^* solves the adjoint problem

$$\begin{cases} \Delta u_n^*(\omega;\cdot) + k_0^2 \overline{\varepsilon_r} u_n^*(\omega;\cdot) = 0 & \text{in } D \backslash \Gamma(\omega), \\ u_n^*(\omega;0,x_2) = u_n^*(\omega;\Lambda,x_2), & 0 < x_2 < b, \\ u_n^*(\omega;x_1,0) = 0, & 0 < x_1 < \Lambda, \\ \dfrac{\partial u_n^*}{\partial x_2}(\omega;x_1,b) = T^*(u_n^*(\omega;x_1,b)) + e^{i\kappa_n x_1} & 0 < x_1 < \Lambda, \\ (u_n^*)_+(\omega;x_1,f(\omega,x_1)) = (u_n^*)_-(\omega;x_1,f(\omega,x_1)) & 0 < x_1 < \Lambda, \\ (\partial_\nu u_n^*)_+(\omega;x_1,f(\omega,x_1)) = (\partial_\nu u_n^*)_-(\omega;x_1,f(\omega,x_1)) & 0 < x_1 < \Lambda. \end{cases} \tag{3.4}$$

In the above theorem, $[u_n^* \bar{u}]|_{(x_1,f)}$ denotes the restriction of $u_n^* \bar{u}$ to the surface $\Gamma(\omega)$. T^* is the adjoint operator of T such that

$$\langle Tu, v \rangle = \langle u, T^* v \rangle,$$

where $\langle \cdot, \cdot \rangle$ stands for the inner product over the function space $L^2(0,\Lambda)$. We postpone the proof of the theorem to Section 3.3.

It now follows that the gradient of the cost function $J(\alpha)$ is given by

$$\nabla_\alpha J = \int_\Omega \nabla_\alpha R(\omega, f)\, dP(\omega). \tag{3.5}$$

We apply the Monte-Carlo method for sampling over the probability space Ω in the above formula. From (3.3), the calculation of $\nabla_\alpha R$ requires the evaluation of the gradient $\nabla_\alpha f$, the solution of the forward scattering problem u and the solution of the adjoint problem u_n^*. Note that $\nabla_\alpha f$ can be calculated directly from the Karhunen–Loève expansion (2.9). The forward scattering problem (2.8) and the adjoint problem (3.4) are solved by the finite element method [6].

3.3 Proof of Theorem 3.1

We first derivate the shape derivative $\nabla_f R$. To this end, one needs to derive the perturbation of the reflectivity, δR, due to the perturbation of the interface by δf. This can be obtained by the following two lemmas.

Lemma 3.2. Let the interface f be perturbed by δf, and $\delta\varepsilon_r$ be the change of the permittivity due to the perturbation of the interface. Then for any test function $v \in L^2(D)$, there holds

$$(v, \delta\varepsilon_r) = \int_0^\Lambda v(x_1, f(x_1))\, \overline{(\varepsilon_{r,1} - \varepsilon_{r,2})} \cdot \delta f\, dx.$$

Proof Let the new interface be denoted by $f^\delta := f+\delta f$. First, it is observed that for any test function $v\in L^2(D)$, the inner product

$$(v,\delta\varepsilon_r) := \int_D v(x)\,\overline{\delta\varepsilon_r}(x)\,dx = \int_{\text{symdiff}(D_1,D_1^\delta)} v(x)\,\overline{\delta\varepsilon_r}(x)\,dx.$$

Here D_1 and D_1^δ are the corresponding absorbing layers with the interfaces f and f^δ respectively, and the symmetric difference of two sets D_1 and D_1^δ is given by

$$\text{symdiff}(D_1,D_1^\delta) = (D_1\cup D_1^\delta)\setminus(D_1\cap D_1^\delta).$$

Now in view of the fact that the relative permittivity of the absorbing and TCO layers are $\varepsilon_{r,1}$ and $\varepsilon_{r,1}$ respectively, the above inner product can be simplified as

$$(v,\delta\varepsilon_r) = \int_0^\Lambda v(x_1,f(x_1))\,\overline{(\varepsilon_{r,1}-\varepsilon_{r,2})}\cdot\delta f\,dx$$

for an infinitesimal δf. □

Lemma 3.3. Let δR be the change of the reflectivity R due to the perturbation of the interface by δf, and $\delta\varepsilon_r$ be the perturbation of the relative permittivity. Then

$$\delta R = \frac{2k_0^2}{\Lambda}\sum_{n\in\mathcal{N}}\frac{\eta_n}{\eta_0}\text{Re}\Big[(\hat{u}_n(\omega;b)-\alpha_n e^{-ik_1 b})\cdot\int_D\bar{\delta\varepsilon}_r\bar{u}u_n^*\,dx\Big]+O(\delta f^2),$$

where $\alpha_0=1$ and $\alpha_n=0$ if $n\neq 0$. u and u_n^* is the solution to the forward problem (2.8) and the adjoint problem (3.4), respectively.

Proof For the perturbed interface $f^\delta := f+\delta f$ so that the permittivity in the solar cell becomes $\varepsilon_r^\delta := \varepsilon_r+\delta\varepsilon_r$, the reflectivity at sample ω is

$$\begin{aligned} R^\delta(\omega,f) &= \sum_{n\in\mathcal{N}}\frac{\eta_n}{\eta_0}|r_n+\delta r_n|^2 \\ &= \sum_{n\in\mathcal{N}}\frac{\eta_n}{\eta_0}\Big\{|r_n|^2+2\text{Re}[r_n\overline{\delta r_n}]+|\delta r_n|^2\Big\} \\ &= R(\omega,f)+2\sum_{n\in\mathcal{N}}\frac{\eta_n}{\eta_0}\text{Re}[r_n\overline{\delta r_n}]+O(\delta f^2). \end{aligned}$$

We see that the perturbation of the reflectivity is

$$\delta R = 2\sum_{n\in\mathcal{N}}\frac{\eta_n}{\eta_0}\text{Re}[r_n\overline{\delta r_n}]+O(\delta f^2). \tag{3.6}$$

For each term $r_n\overline{\delta r_n}$, by virtue of (3.1), it follows that

$$r_n\overline{\delta r_n} = \begin{cases} \hat{u}_n(\omega;b)\cdot\dfrac{1}{\Lambda}\displaystyle\int_0^\Lambda e^{i\kappa_n x_1}\,\overline{\delta u(\omega;x_1,b)}\,dx_1, & n\neq 0 \\ \big(\hat{u}_n(\omega;b)-e^{-ik_1 b}\big)\cdot\dfrac{1}{\Lambda}\displaystyle\int_0^\Lambda e^{i\kappa_n x_1}\,\overline{\delta u(\omega;x_1,b)}\,dx_1, & n=0. \end{cases} \tag{3.7}$$

In the above, δu denotes the perturbation of the total field.

From a perturbation analysis, it is clear that δu solves the following boundary value problem:

$$\begin{cases} \Delta\delta u(\omega;\cdot)+k_0^2\varepsilon_r\delta u(\omega;\cdot)=-k_0^2\delta\varepsilon_r u(\omega;\cdot) & \text{in } D\backslash\Gamma(\omega), \\ \delta u(\omega;0,x_2)=\delta u(\omega;\Lambda,x_2), & 0<x_2<b, \\ \delta u(\omega;x_1,0)=0, & 0<x_1<\Lambda \\ \dfrac{\partial\delta u}{\partial x_2}(\omega;x_1,b)=T(\delta u(\omega;x_1,b)) & 0<x_1<\Lambda, \\ (\delta u)_+(\omega;x_1,f(\omega,x_1))=(\delta u)_-(\omega;x_1,f(\omega,x_1)) & 0<x_1<\Lambda, \\ (\partial_\nu\delta u)_+(\omega;x_1,f(\omega,x_1))=(\partial_\nu\delta u)_-(\omega;x_1,f(\omega,x_1)) & 0<x_1<\Lambda. \end{cases} \tag{3.8}$$

By multiplying the PDE in the adjoint problem (3.4) by $\overline{\delta u}$ and the PDE in (3.8) by $\overline{u_n^*}$, and integrating over the domain D_1 and D_2 respectively, it follows that

$$\int_{D_j}(\Delta u_n^*+k_0^2\overline{\varepsilon_r}u_n^*)\,\overline{\delta u}-u_n^*\,\overline{(\Delta\delta u+k_0^2\varepsilon_r\delta u)}\,dx=\int_{D_j}u_n^*k_0^2\overline{\delta\varepsilon_r u}\,dx,\quad j=1,2.$$

An application of the Green's second identity for the left-hand sides and adding the above two equations together yields

$$\begin{aligned}&\int_{\Gamma(\omega)}(\partial_\nu u_n^*)_-\overline{(\delta u)}_--(u_n^*)_-\overline{(\partial_\nu\delta u)}_-ds+\int_{\Gamma(\omega)}(u_n^*)_+\overline{(\partial_\nu\delta u)}_+-(\partial_\nu u_n^*)_+\overline{(\delta u)}_+ds\\&+\int_0^\Lambda e^{i\kappa_n x}\,\overline{\delta u(\omega;x_1,b)}\,dx_1=k_0^2\int_{D_1\cup D_2}\bar\delta\varepsilon_r\bar u u_n^*\,dx,\end{aligned}$$

where we have used the boundary conditions in (3.4) and (3.8). This can be further reduced to the following from the continuity condition along the interface $\Gamma(\omega)$:

$$\int_0^\Lambda e^{i\kappa_n x}\,\overline{\delta u(\omega;x_1,b)}\,dx_1=k_0^2\int_D\bar\delta\varepsilon_r\bar u u_n^*\,dx.$$

Therefore, by substituting into (3.7), we have

$$r_n\overline{\delta r_n}=\begin{cases}\hat u_n(\omega;b)\cdot\dfrac{k_0^2}{\Lambda}\displaystyle\int_D\bar\delta\varepsilon_r\bar u u_n^*\,dx, & n\neq0,\\ \big(\hat u_n(\omega;b)-e^{-ikb}\big)\cdot\dfrac{k_0^2}{\Lambda}\displaystyle\int_D\bar\delta\varepsilon_r\bar u u_n^*\,dx, & n=0.\end{cases} \tag{3.9}$$

Consequently, in light of (3.6), the perturbation of the reflectivity is expressed by

$$\delta R=\frac{2k_0^2}{\Lambda}\sum_{n\in\mathcal{N}}\frac{\eta_n}{\eta_0}\mathrm{Re}\Big[(\hat u_n(\omega;b)-\alpha_n e^{-ik_1b})\cdot\int_D\bar\delta\varepsilon_r\bar u u_n^*\,dx\Big]+O(\delta f^2).$$

□

Proof of Theorem 3.1: Suppose that the interface f be perturbed by δf. A combination of Lemmas 3.2 and 3.3 leads to the perturbation of reflectivity, which is given by

$$\delta R = \frac{2k_0^2}{\Lambda}\sum_{n\in\mathcal{N}}\frac{\eta_n}{\eta_0}\mathrm{Re}\Big[(\hat{u}_n(\omega;b)-\alpha_n e^{-ik_1 b})\cdot\overline{(\varepsilon_{r,1}-\varepsilon_{r,2})}\cdot\int_0^\Lambda[\bar{u}u_n^*]|_{(x_1,f)}\cdot\delta f\,dx_1\Big]+O(\delta f^2).$$

The desired formula (3.3) for $\nabla_\alpha R$ then follows by the chain rule.

4 Numerical experiments

In this section, we present several numerical examples to demonstrate the efficiency of the numerical algorithms for solving the optimal design problem. The first numerical example tests the accuracy of the finite element solver for the scattering problem, whereas in the second and third examples, we test the convergence of the optimization algorithm, and compare the absorbance of the solar cell using the obtained optimal random textures with that of the existing commercialized substrates at two different optical wavelengths.

In all examples, the height of the reference surface, or equivalently the average thickness of the absorbing layer, is set as $a=300$ nm, and the size of the periodic cell $\Lambda=1500$ nm. The number of random samples used in the Monte Carlo sampling is set as $M=1000$, and the calculation of derivative $\nabla_\alpha R(\omega)$ for different samples are run in parallel.

Example 1 In this example, we test the accuracy of the numerical solver for the scattering problem. Let us assume that the free space wavelength $\lambda_0=500$ nm. The refractive index is $q_1=2.0$ and $q_2=1.2$ in D_1 and D_2, respectively.

We first consider the case when the interface between the TCO layer and absorbing layer is free of random perturbation. Then for a normal incident time–harmonic plane wave $u^i=e^{-ik_0q_2x_2}$, where k_0 is the free-space wavenumber, the analytical solution for the total field of the scattering problem (2.1) takes the form of

$$u(x)=\begin{cases} e^{-ik_0q_2x_2}+c_2e^{ik_0q_2x_2}, & x\in D_2,\\ \\ c_1(e^{ik_0q_1x_2}-e^{-ik_0q_1x_2}), & x\in D_1,\end{cases}$$

where

$$c_1=\frac{2q_2e^{-ik_0q_2a}}{q_2(e^{ik_0q_1a}-e^{-ik_0q_1a})-q_1(e^{ik_0q_1a}+e^{-ik_0q_1a})},$$

and

$$c_2=\frac{(e^{ik_0q_1a}-e^{-ik_0q_1a})}{e^{ik_0q_1a}}\cdot c-e^{-i2k_0q_2a}.$$

We apply the linear finite element to solve the scattering problem with the mesh size $\Delta=12$ nm,6 nm,3 nm,1.5 nm, and the corresponding L^2-norm of numerical errors are

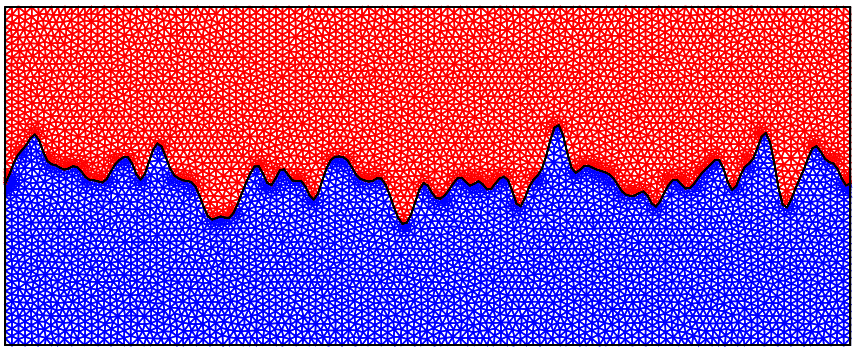

Figure 5: Triangulation of the domain D with $\Delta = 12\,\mathrm{nm}$.

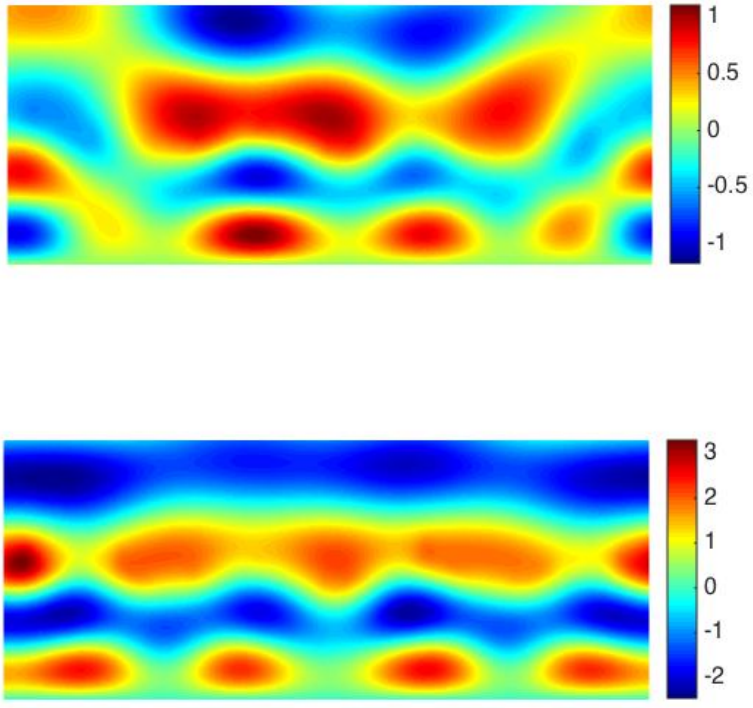

Figure 6: Real (top) and imaginary part (bottom) of the total field with $\Delta = 3\,\mathrm{nm}$.

Table 1: L^2-norm of the error for the numerical solution at various mesh sizes and the corresponding convergence order.

Δ	12 nm	6 nm	3 nm	1.5 nm
$\|\|u-u_\Delta\|\|_{L^2(D)}$	0.2224	0.0539	0.0137	0.0034
convergence order		2.04	1.98	2.01

shown in Table 1. It is observed the convergence order of numerical method is about 2, which is consistent with the convergence theory of the linear finite element method.

Next we consider a rough surface, which is one realization of the random surface with the RMS height $\sigma = 30$ nm and the correlation length $\ell = 24$ nm. The domain D is decomposed with the mesh size $\Delta = 12\,\text{nm}, 6\,\text{nm}, 3\,\text{nm}, 1.5\,\text{nm}$, respectively. The triangulation with $\Delta = 12\,\text{nm}$ is plotted in Figure 5. To test the convergence of the PDE solver, we choose the numerical solution $\tilde{u}$ with the mesh size $\Delta = 0.6\,\text{nm}$ as the reference solution, and compute the L^∞-norm error $||\tilde{u}-u_\Delta||_{L^\infty}$ along the boundary $x_2 = b$ for the four different triangulations defined above. This is shown in Table 2, which clearly confirms the convergence of the finite element method. To illustrate the scattering effect by the rough surface, we also plot the total field for the scattering problem with $\Delta = 3\,\text{nm}$ in Figure 6.

Table 2: $||\tilde{u}-u_\Delta||_{L^\infty}$ for various mesh sizes along the boundary $x_2 = b$, where $\tilde{u}$ is the reference solution obtained with $\Delta = 0.6\,\text{nm}$.

Δ	12 nm	6 nm	3 nm	1.5 nm
$\|\|\tilde{u}-u_\Delta\|\|_{L^\infty}$	0.2840	0.0738	0.0112	0.0059

Example 2 Assume that the free space wavenlength $\lambda_0 = 650$ nm. The refractive index of the TCO layer is 1.915, or equivalently, its relative permittivity $\varepsilon_{r,1} = 3.667$ [11,17,27]. The refractive index of the absorbing layer is set as $4.2 + 0.045i$ when $\lambda_0 = 650$ nm [31]. This implies that the relative permittivity $\varepsilon_{r,2} = 17.6380 + 0.3780i$. We apply the steepest decent algorithm to solve the optimization problem (3.2), where the gradient is computed via formulas (3.3) and (3.5).

Figure 7 demonstrates the decrease of the cost function $J(\alpha)$ for each iteration when the Armijo's line search method is used. It takes 7 iterations to achieve a minimum of $J(\alpha)$, and the RMS height and the correlation length for all iterations are shown in Table 3. The obtained optimal RMS height and the correlation length are σ=65.64 nm and ℓ=36.08 nm, respectively. Figure 8 shows one realization of random surfaces with the optimal statistical parameters, and Figure 9 is the corresponding total field after the scattering by the rough surface.

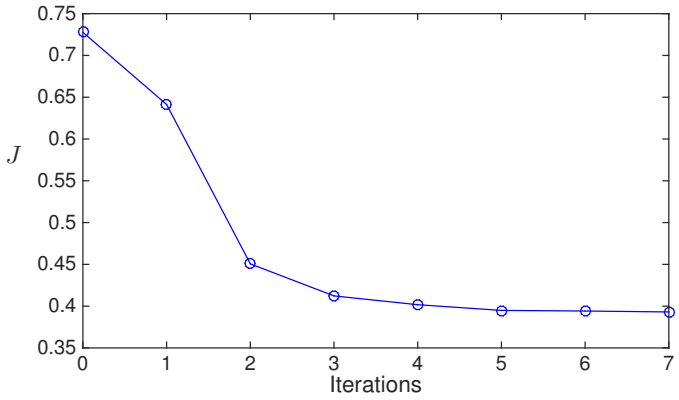

Figure 7: The cost function $J(\alpha)$ for all iterations.

Table 3: The values of σ and ℓ for all iterations.

Iteration	0	1	2	3	4	5	6	7
σ (nm)	15	23.65	44.45	57.43	62.96	65.21	65.48	65.64
ℓ (nm)	30	30.47	33.18	34.02	34.33	36.07	36.07	36.08

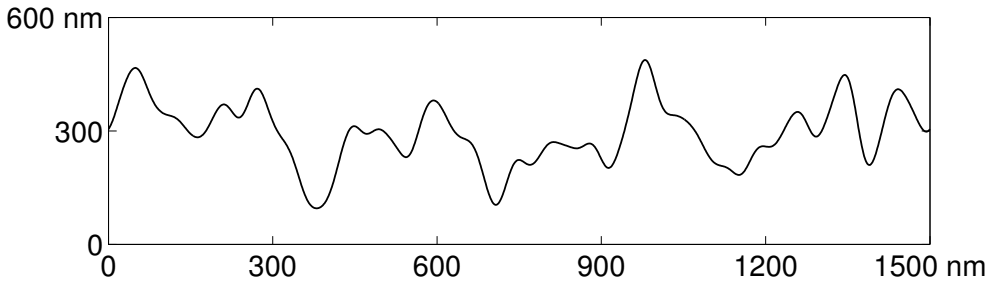

Figure 8: Realization of the random surface with the obtained optimal statistical parameters.

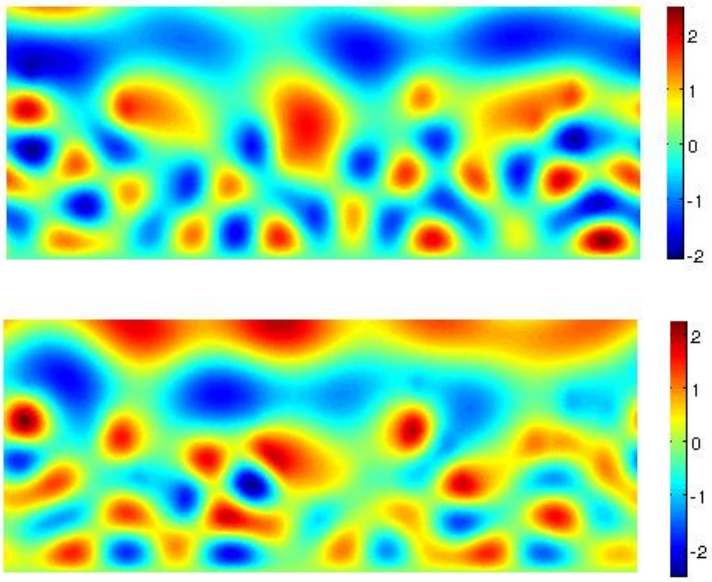

Figure 9: Real (top) and imaginary part (bottom) of the total field for the scattering by the surface shown in Figure 8.

It can be calculated that $\mathbb{E}[A]$, the average absorptance of the solar cell with the obtained optimal random surface texture, is about 0.61. As a comparison, we also compute the absorptance for the solar cell with a flat surface (with no random texture) and the Asahi-U substrate, and collect all values in Table 4. The Asahi-U substrate, which has a RMS height of 35 nm and a correlation length of 160 nm, has been shown to yield the highest efficiency among the three commercialized solar cells (Namely, Asahi-U, Jülich, and Neuchătel cells) [27]. It is seen that the absorptance for a flat surface is only 0.24. Hence the absorption enhancement is 2.6 when the optimal randomized textures are employed along the interface of the TCO and the absorbing layers. By a direct calculation, the Asahi-U cell yields an average absorptance of 0.45. Therefore, the random textures obtained from solving optimization problem (3.2) yield a much higher absorptance than the Asahi-U cell. It should be pointed out that the current comparison is performed for two dimensional structures. Further investigation in three dimensions still need to be carried out, and this will be reported elsewhere.

For comparison purpose, we also plot one realization of the Asahi-U surface and the corresponding total field in Figure 10 and Figure 11, respectively. Clearly, the obtained optimal surfaces have smaller correlation length than the Asahi-U surface, and are much rougher as a result. On the other hand, the optimal RMS height are larger than the Asahi-U surface. Consequently, as observed from Figure 9 and Figure 11, the multiple scattering effect becomes more manifested for the wave field of the optimal surfaces. This may lead to a higher obsorptance for the realization of the optimal surface, which has a value of 0.64, compared to 0.54 for the Asahi-U surface.

Table 4: The absorptances of solar cells with three different types of surfaces.

	flat surface	Asahi-U substrate	optimal surface
σ (nm)	0	35	65.64
ℓ (nm)		160	36.08
$\mathbb{E}[A]$	0.24	0.45	0.62

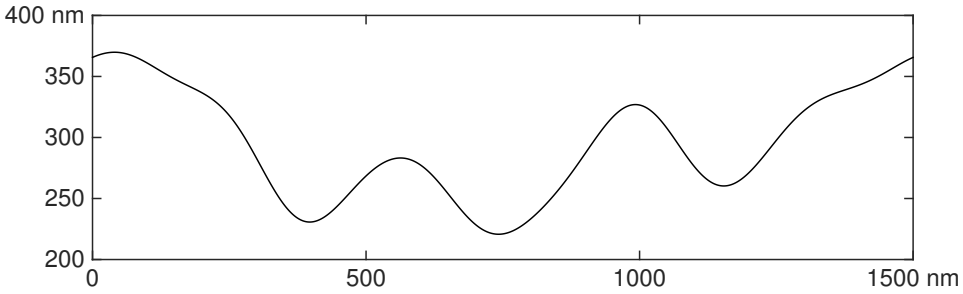

Figure 10: Realization of the Asahi-U random surface in one cell.

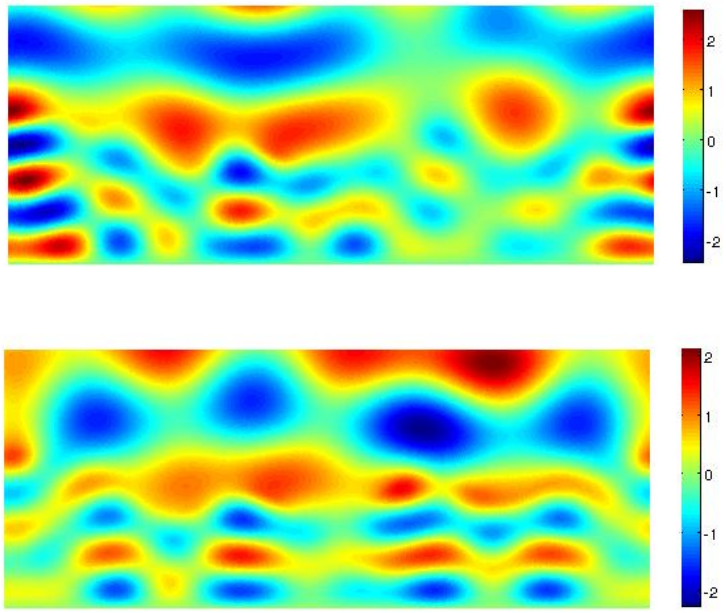

Figure 11: Real (top) and imaginary part (bottom) of the total field for the scattering by the Asahi-U surface.

Example 3 In this example, we consider the optimization when the free space wavelength $\lambda_0 = 720$ nm. The refractive index of the absorbing layer is $4+0.0035i$ [31]. Figure 12 demonstrates the decrease of the cost function $J(\alpha)$ during the steepest descent iteration, and Table 5 are the corresponding σ and ℓ values. We see that the optimal correlation length is close to that obtained for $\lambda_0 = 650$ nm, while the RMS height are quite different for two cases. Numerical studies at other wavelengths also show that the optimal correlation length is close to 40 nm. This is very useful in providing guidance to solve the broadband optimal design problem, which is currently explored. One realization of random surfaces with the obtained RMS height and the correlation length is plotted Figure 13, and Figure 14 shows the corresponding total field after the scattering by the rough surface. Again, the multiple scattering effect for the wave field of the optimal surface is more manifested than the Ashahi-U cell (see Figure 15) due to the roughness of the former, and the aborptance is much higher (with a value of 0.28, compared to 0.04 for the Ashahi-U cell).

The average absorptances of solar cells with three types of surfaces are shown in Table 6. We see that the average absorptance of the solar cell with the obtained optimal random surface texture is about 0.3, while the absorptance of the cell with a flat surface is only 0.02. That is, an absorption enhancement of 15 is gained. On the other hand, the Asahi-U substrate gives rise to an average absorptance of 0.11. Hence the absorption efficiency for the solar cell with the random textures obtained by solving the optimization problem (3.2) is much higher than that of the Asahi-U cell.

Table 5: The values of σ and ℓ for all iterations.

Iteration	0	1	2	3	4	5	6
σ (nm)	60	54.40	46.40	36.07	22.37	22.87	22.58
ℓ (nm)	30	28.67	32.60	34.69	36.07	36.12	36.26

Table 6: The absorptances of solar cells with three different types of surfaces.

	flat surface	Asahi-U substrate	optimal surface
σ (nm)	0	35	22.58
ℓ (nm)		160	36.26
$\mathbb{E}[A]$	0.02	0.11	0.3

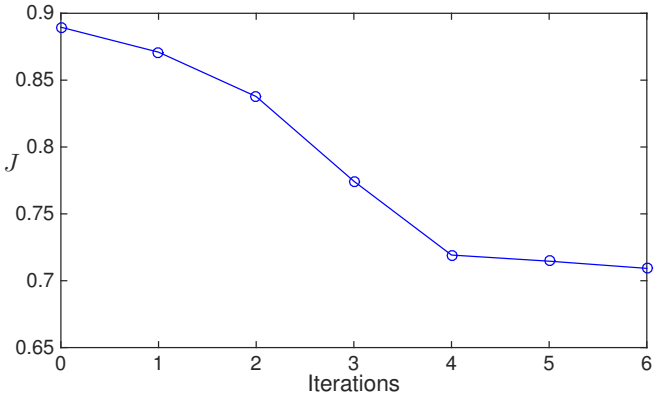

Figure 12: The cost function $J(\alpha)$ for all iterations.

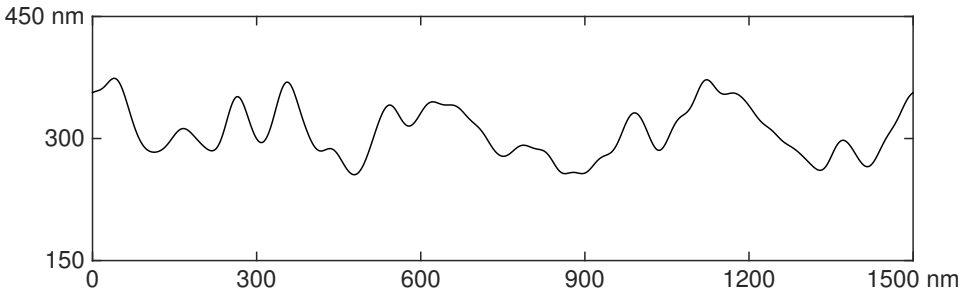

Figure 13: Realization of the random surface with the obtained optimal statistical parameters.

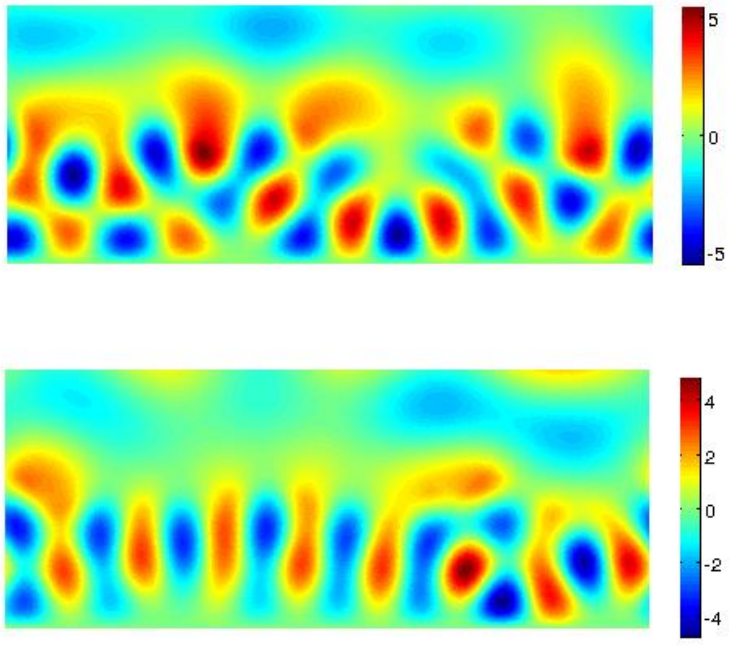

Figure 14: Real (top) and imaginary part (bottom) of the total field for the scattering by the surface shown in Figure 13.

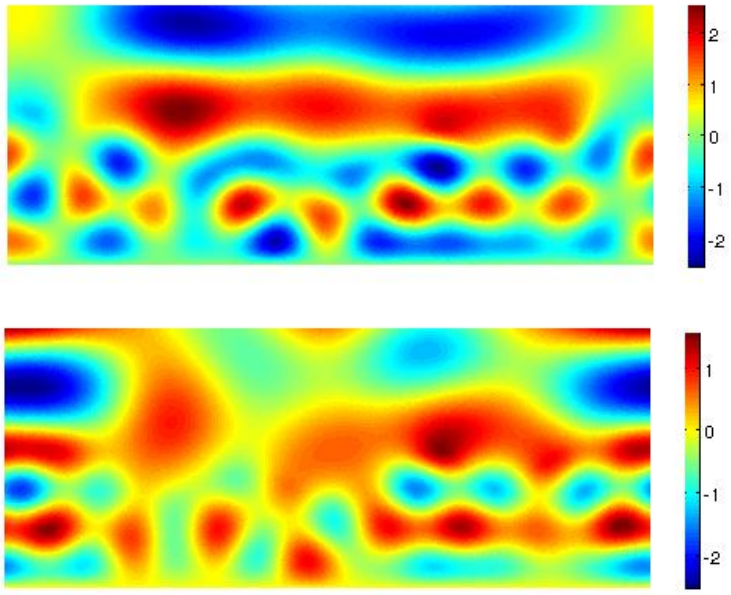

Figure 15: Real (top) and imaginary part (bottom) of the total field for the scattering by the Asahi-U surface.

5 Conclusions

In this paper, we have formulated the optimal design problem for random surface textures in thin-film solar cells and presented a gradient-based algorithm with the adjoint state method to solve the problem numerically. It is shown that the optimal random textures obtained numerically would yield a significant absorption enhancement. The mathematical and numerical investigation presented here is the first study along this research direction and we are currently exploring further to answer the following questions. In terms of the formulation of the optimal design problems, first, in addition to optimize the average of the absorptance, one may need to optimize its variance so that the efficiency of all realization of optimal random surface would gain certain stability. Second, due to the broadband nature of optical light, it would be desirable to perform optimization over a band of optical frequency. Finally, the interface between the absorbing layer and perfect reflector can also be textured in a random manner and is also subject to optimization. In terms of the numerical approach, more efficient random sampling technique such as multi-level Monte Carlo method will be employed. In addition, the numerical simulations and the optimal design procedures will be carried out for the three-dimensional models.

Acknowledgment

The work of G. Bao is supported in part by a NSFC Innovative Group Fun (No.11621101), an Integrated Project of the Major Research Plan of NSFC (No. 91630309), and an NSFC A3 Project (No. 11421110002), and the Fundamental Research Funds for the Central Universities, the work of YC was partially supported by the NSF grant DMS-1620150, and the work of JL was partially supported by the NSF grant DMS-1417676. JL gratefully acknowledges the support and hospitality provided by the IMA in University of Minnesota during his visit and when part of this project is performed.

References

[1] C. Battaglia, et al. *Light trapping in solar cells: can periodic beat random?*, ACS Nano, **6** (2012): 2790-2797.

[2] G. Bao, D. Dobson, and J. Cox, *Mathematical studies in rigorous grating theory*. J. Opt. Soc. Amer. A, **12** (1995), 1029-1042.

[3] G. Bao and Y. Wang, *Optimal design of antireflection coatings with different metrics*, J. Opt. Soc. Am. A, **30** (2013), 656-662.

[4] P. Bermel *et al*, *Improving thin-film crystalline silicon solar cell efficiencies with photonic crystals*, Opt. Express **15** (2007), 16986.

[5] A. BONNET-BENDHIA AND F. STARLING, *Guided waves by electromagnetic gratings and non-uniqueness examples for the diffraction problem*, Math. Meth. Appl. Sci., **17** (1994), 305-338.

[6] S. Brenner and R. Scott, *The Mathematical Theory of Finite Element Methods*, Texts Applied Mathematics (Vol. 15), Springer Science & Business Media, 2007.

[7] A. Čampa, J. Krč, and M. Topič, *Analysis and optimisation of microcrystalline silicon solar cells with periodic sinusoidal textured interfaces by two-dimensional optical simulations*, J. Appl. Phys., **105** (2009), 083107.

[8] Y. Cao and D. Stanescu, *Shape optimization for noise radiation problems*, Comput. & Math. Appl., **44** (2002), 1527-1537.

[9] Y. Cao M. Y. Hussaini , and H. Yang, *Numerical optimization of radiated engine noise with uncertain wavenumbers*, Int. J. Numer. Anal. Mod., **4** (2007), 392-401.

[10] M. Delfour and and J. Zolésio, *Shapes and geometries: Metrics, analysis, differential calculus, and optimization*, Advances in Design and Control, SIAM, **22** (2011).

[11] S. Fahr, C. Rockstuhl, and F. Lederer, *Engineering the randomness for enhanced absorption in solar cells*, Appl. Phy. Lett. **92** (2008): 171114.

[12] V. Ferry, et al. *Optimized spatial correlations for broadband light trapping nanopatterns in high efficiency ultrathin film a-Si: H solar cells*, Nano Lett., **11** (2011), 4239-4245.

[13] J. C. Goldschmidt *et al*, *Increasing the efficiency of fluorescent concentrator systems*, Sol. Energy Mat. Sol. Cells, **93** (2009), 176-182.

[14] G. Gunzburger and H. Kim, *existence of an optimal solution of a shape control problem for the stationary Navier-Stokes equations*, SIAM J. Control Optim., **36** (1998), 895-909.

[15] J. Haslinger and R. Mäkinen, *Introduction to Shape Optimization: Theory, Approximation, and Computation*, Society for Industrial and Applied Mathematics, 2003.

[16] M. Hinze *et al.*, *Optimization with PDE Constraints*, Mathematical Modeling: Theory and Applications (Vol. 23), Springer Science & Business Media, 2008.

[17] P. Kowalczewski, M. Liscidini, and L. Andreani, *Engineering Gaussian disorder at rough interfaces for light trapping in thin-film solar cells*, Opt. Lett., **37** (2012), 4868-4870.

[18] O. Kluth *et al Texture etched ZnO: Al coated glass substrates for silicon based thin film solar cells*, Thin Solid Films, **351** (1999), 247-253.

[19] C. Lalau-Keraly, S. Bhargava, O. Miller, and E. Yablonovitch, *Adjoint shape optimization applied to electromagnetic design*, Opt. Exp., **21** (2013), 21693-21701.

[20] G. Lord, C. Powell, and T. Shardlow, *An Introduction to Computational Stochastic PDEs*, Cambridge University Press, 2014.

[21] A. McEvoy et al., eds. *Practical Handbook of Photovoltaics: Fundamentals and Applications*, Elsevier, 2003.

[22] J. Müller, R. Bernd, J. Springer, and M. Vanecek, *TCO and light trapping in silicon thin film solar cells*, Solar Energy **77** (2004), 917-930.

[23] S. Nicolay *et al*, *Control of LPCVD ZnO growth modes for improved light trapping in thin film silicon solar cells* Solar Energy Materials and Solar Cells, **95** (2011), 1031-1034.

[24] J. Nocedal and S. Wright, *Numerical Optimization* (Second edition), Springer New York, 2006.

[25] J. A. Ogilvy, *Theory of Wave Scattering from Random Rough Surfaces*, Adam Hilger, 1991.

[26] J. Poortmansand and V. Arkhipov, eds. *Thin film solar cells: fabrication, characterization and applications*, Vol. 5, John Wiley & Sons, 2006.

[27] C. Rockstuhl, et al., *Comparison and optimization of randomly textured surfaces in thin-film solar cells*, Opt. Exp., **18** (2010), A335-A341.

[28] C. Rockstuhl and F. Lederer, *Photon management by metallic nanodiscs in thin film solar cells*, Appl. Phys. Lett., **94** (2009), 213102.

[29] X. Sheng, S. Johnson, J. Michel, and L. Kimerling, *Optimization-based design of surface textures for thin-film Si solar cells*, Opt. Exp., **19** (2011), A841-A850.

[30] J. Sokolowski and J. P. Zolesio, Introduction to Shape Optimization, Springer Berlin Heidelberg, 1992.

[31] M. Zeman *et al*, Optical modeling of a-Si:H solar cells with rough interfaces: Effect of back contact and interface roughness, J. Appl. Phys., **88** (2000), 6436-6443.